Reduced order modelling for turbomachinery shape design

Andrea Ferrero, Angelo Iollo, Francesco Larocca

ARTICLE TEMPLATE

Reduced order modelling for turbomachinery shape design

Andrea Ferrero[a], Angelo Iollo [b,c,d] and Francesco Larocca[a]

[a]DIMEAS, Politecnico di Torino, Torino, Italy;
[b]MEMPHIS Team, INRIA Bordeaux Sud-Ouest, Talence, France;
[c]IMB, Université de Bordeaux, Talence, France;
[d]CNRS, Talence, France

ARTICLE HISTORY
Compiled September 20, 2019

ABSTRACT
Reduced order modelling (ROM) techniques allow to reduce the cost of shape optimisation problems. In the present work, the compressible turbulent flow around a gas turbine profile is studied by a Discontinuous Galerkin (DG) scheme. The simulations are accelerated by the combination of two existing ROM approaches: Domain Decomposition and Local Proper Orthogonal Decomposition in a DG (LPOD-DG) framework. In particular, the focus is fixed on the airfoil suction side which is deformed while the pressure side remains fixed. The proposed method allows to reduce significantly the number of degrees of freedom in the simulation. The method is evaluated by performing a set of random predictions for shapes not included in the training database and comparing the obtained results with high-fidelity simulations. The approach is also compared to a p-adaptive scheme. Finally, the use of an automatic adaptive technique is investigated in order to improve the prediction accuracy at runtime.

KEYWORDS
Reduce Order Modelling; POD; Turbomachinery; Shape optimisation; Discontinuous Galerkin; RANS

1. Introduction

The design of aeronautic gas turbines is based on multidisciplinary approaches which require to find a compromise between the requirements imposed by several disciplines: aerodynamics, structural mechanics, aeroacoustics represent some examples. For this reason, the design process is usually performed by means of iterative cycles in which hundred or thousands of different configurations are evaluated. In order to maintain the design cost under an acceptable level it is mandatory to introduce cheap low-order models in the preliminary steps of the process while expensive high-fidelity models can be afforded only when the design is almost fixed.
In the present work the use of Reduced Order Modelling (ROM) techniques is investigated in order to reduce the cost required by the simulation of the flow field around a gas turbine airfoil.
Several ROM methodologies are available in the literature. They usually rely on a two steps approach: an offline phase during which high-fidelity data are collected by

CONTACT A. Ferrero. Email: andrea_ferrero@polito.it

means of experimental investigations or accurate numerical simulations and an online phase in which a low-order model trained on the high-fidelity database is called to perform low cost predictions. This idea of exploiting the available data to improve the predictions can be seen as the natural application of machine-learning techniques to engineering simulations: several recent research efforts seem to go in this direction by enriching the physics of the model by means of data-driven corrections (Bai et al. (2017); Mohebujjaman, Rebholz, and Iliescu (2018); Gibou, Hyde, and Fedkiw (2018); Swischuk et al. (2018); Bertram, Othmer, and Zimmermann (2018)).

Several ROM techniques are based on Principal Component Analysis, also known as Proper Orthogonal Decomposition (POD) in fluid mechanics (see from example the pioneering work of Sirovich (1987)). Other possible alternatives fall in the class of Proper Generalised Decomposition (Chinesta, Keunings, and Leygue (2013)), Reduced Basis (Quarteroni, Rozza, and Manzoni (2011); Quarteroni and Rozza (2014)), hierarchical model reduction (Baroli et al. (2017); Aletti, Perotto, and Veneziani (2018), Dynamic Mode Decomposition (Schmid (2010); Noack et al. (2016)) and hyper-reduction (Amsallem et al. (2015)). Another relevant class of ROM techniques is based on the definition of particular interpolation methods: some examples are represented by the Grassmannian interpolation (Amsallem and Farhat (2008)), the Empirical Interpolation Method (Barrault et al. (2004)), the Discrete Empirical Interpolation Method (Chaturantabut and Sorensen (2010)) and the use of active subspaces and response surfaces(Tezzele et al. (2018)).
Finally, some approaches based on domain decomposition have been proposed (Buffoni, Telib, and Iollo (2009); Baiges, Codina, and Idelsohn (2013); Bergmann et al. (2018); Salmoiraghi et al. (2018)). The main idea behind these last techniques is to subdivide the domain in several regions in which different models are employed, usually switching between an high-fidelity and a low-fidelity model.

In this work, the prediction of the flow field around a family of gas turbine airfoils is considered. The flow field is described by the compressible Reynolds Averaged Navier-Stokes (RANS) equations discretised by means of a Discontinuous Galerkin (DG) scheme. The attention is focused on the design of the suction side while the other geometrical features of the airfoil (pressure side shape, leading and trailing edge arcs, inlet and outlet metallic angles) are assumed fixed. The motivation behind the choice of this example is that the shape of the suction side significantly influences the risk of flow separation and so it should be carefully optimised. The fact that part of the geometry remains fixed makes the problem particularly suitable for the application of domain decomposition techniques. In particular, the computational domain will be split in a region with a fixed mesh (close to the pressure side) and a region where the mesh changes according to the shape of the airfoil (close to the suction side). Since a modal DG scheme is used for spatial discretisation, there is great flexibility in the choice of the element basis. In particular, a standard modal basis will be used in the changing mesh region. In contrast, the solution in the elements which belong to the fixed mesh region will be described by a local POD basis trained on a database of high-fidelity solutions, according to the LPOD-DG approach (Ferrero, Iollo, and Larocca (2018)). The ability of the POD algorithm to compress the information allows to reduce significantly the number of degrees of freedom in the fixed mesh region. This approach is similar in spirit to the zonal POD method (Buffoni, Telib, and Iollo (2009); Bergmann et al. (2018)) where the domain is split between a region where the high-fidelity solver is called and a region where the solution is described by global POD

modes. The difference with respect to the present work relies on the fact that here local POD basis are used on each element instead of global modes and the coupling between the different zones does not require the definition of an overlapping region (as proposed by Buffoni, Telib, and Iollo (2009); Bergmann et al. (2018))) but is here automatically managed in the discontinuous Galerkin framework.
Furthermore, the zonal POD method, the LPOD-DG method and their combination presented in this work do not require the introduction of problem-dependent stabilisation terms. In particular, the numerical stability of the DG scheme is here exploited to stabilise the simulations. This makes the predictions more robust with respect to POD-Galerkin approaches in which the stabilisation terms need to be interpolated when new working conditions are evaluated (see for example Weller, Camarri, and Iollo (2009)).

The paper is organised as follows. In Section 2 the physical model and the numerical discretisation are reported. In Section 3 the domain decomposition approach and the LPOD-DG are presented. Finally, in Section 4 the proposed techniques are applied to the shape deformation of a gas turbine blade. Conclusions and future perspectives are reported in Section 6.

2. High-fidelity model

2.1. *Physical model*

The flow field around the turbine airfoil is described by the two-dimensional compressible RANS equations with the Spalart-Allmaras turbulence model. The governing equations are the following:

$$\frac{\partial \boldsymbol{q}}{\partial t} + \nabla \cdot \boldsymbol{F} = \boldsymbol{S} \qquad \boldsymbol{q}, \boldsymbol{S} \in \mathbb{R}^5, \qquad \boldsymbol{F} \in \mathbb{R}^{5\times 2}, \tag{1}$$

where $\boldsymbol{q} = \{\rho, \rho\boldsymbol{u}, E, \rho\tilde{\nu}\}$ is the vector of the conservative variables, $\boldsymbol{F}$ contains the convective and diffusive fluxes and $\boldsymbol{S}$ is a source term (which is non-null only for the Spalart-Allmaras equation). Details of the flux and source terms for the implemented compressible form of the Spalart-Allmaras model can be found in Allmaras and Johnson (2012).

Here, P, ρ, E, $\boldsymbol{u}$, ν and $\hat{\nu}$ represent pressure, density, total energy per unit volume, velocity, kinematic viscosity and modified eddy viscosity, respectively. The flow is expected to follow the ideal gas law. The dynamic viscosity is assumed constant with temperature and the specific heat ratio is set equal to $\gamma = 1.4$. The heat flux $\boldsymbol{q}$ is computed by means of the Fourier law. The Prandtl number and the turbulent Prandtl number are set to $Pr = 0.72$ and $Pr_t = 0.9$, respectively.
In the following the isentropic Mach number M_{is} will be considered for the characterisation of the flow field around the blade profile. It is defined by the following relation:

$$\frac{P_{in}^o}{P} = \left(1 + \frac{\gamma - 1}{2} M_{is}^2\right)^{\frac{\gamma}{\gamma-1}}, \tag{2}$$

where P_{in}^o is the inlet total pressure.

2.2. *Discontinuous Galerkin spatial discretisation*

The spatial discretisation is performed by means of a modal DG scheme. This choice is characterised by great flexibility since it allows to use different basis functions in each element without any constrain imposed by the element shape (Bassi et al. (2012)). Consider the computational domain Ω. It is discretised by a set of non-overlapping elements Ω_e. In each element the solution is assumed to belong to a finite dimensional functional space V_h which is spanned by polynomial functions of degree at most p continuous only inside each element. Let $\phi(\boldsymbol{x})$ be a modal basis with size N_e for V_h. The conservative variables vector $\boldsymbol{q} \in \mathbb{R}^5$ is described in terms of basis functions $\phi(\boldsymbol{x})$ and degrees of freedom $\tilde{\boldsymbol{q}} \in \mathbb{R}^{5\times N_e}$:

$$q_l(\boldsymbol{x},t) = \sum_{i=1}^{N_e} \tilde{q}_{li}(t)\phi_i(\boldsymbol{x}) \qquad\qquad 1 \leq l \leq 5. \tag{3}$$

The modal basis functions are here obtained by means of the modified Gram-Schmidt orthonormalisation applied to a set of monomials defined in the physical space, following the approach of Bassi et al. (2012). The size of the basis is $N_e = \frac{(p+1)(p+2)}{2}$, for both triangular and quadrilateral elements since this approach can be applied to generally shaped elements.
The space discretisation is completed by the multiplication of Eq. 1 by an arbitrary test function belonging to V_h and by the use of integration by parts:

$$\sum_{i=1}^{N_e} \frac{d\tilde{q}_{li}}{dt} \int_{\Omega_e} \phi_i\phi_j d\Omega = \int_{\Omega_e} \sum_{m=1}^{2} \frac{\partial \phi_j}{\partial x_m} F_{lm} d\Omega - \int_{\partial\Omega_e} \phi_j \sum_{m=1}^{2} \bar{F}_{lm} n_m d\sigma + \int_{\Omega_e} S_l \phi_j d\Omega, \tag{4}$$

where $1 \leq l \leq 5$, $1 \leq j \leq N_e$ and $\boldsymbol{n}$ represents the outward pointing unit normal vector. The convective and diffusive contributions to the numerical fluxes $\bar{F}_{lm}$ at the interfaces between elements are computed according to Pandolfi (1984) and Ferrero, Larocca, and Puppo (2015), respectively.

2.3. *Implicit time integration*

The time integration of Eq. 4 is performed by means of the backward implicit Euler method which allows to accelerate the convergence to the steady state solution following the pseudo-transient continuation strategy proposed by Bassi et al. (2010). In particular, this strategy allows to automatically increase the Courant Friedrich Lewis (CFL) number which defines the time step size as the residuals decrease. For the present work, the CFL number was allowed to automatically vary from 1 to 10^4.
The total number of degrees of freedom can be evaluated as $N_{DOF} = \sum_{\Omega_e \in \Omega} 5N_e$. The application of the backward Euler method to Eq.1 leads to the following set of equations which has to be solved at each time step k:

$$[\boldsymbol{M}]\frac{\tilde{\boldsymbol{Q}}^{k+1} - \tilde{\boldsymbol{Q}}^{k}}{\Delta t} = \tilde{\boldsymbol{R}}(\tilde{\boldsymbol{Q}}^{k}) + \tilde{\boldsymbol{J}}(\tilde{\boldsymbol{Q}}^{k})(\tilde{\boldsymbol{Q}}^{k+1} - \tilde{\boldsymbol{Q}}^{k}), \tag{5}$$

where $\tilde{\boldsymbol{Q}} \in R^{N_{DOF}}$ is the global vector of unknown, $\tilde{\boldsymbol{J}} \in R^{N_{DOF}\times N_{DOF}}$ is the jacobian matrix, the vector $\tilde{\boldsymbol{R}} \in \boldsymbol{R}^{\boldsymbol{N_{DOF}}}$ is obtained by the right hand side of Eq. 4, Δt is

the time step size and the matrix $[\boldsymbol{M}]$ is the identity because the element bases are orthonormal and a formulation based on conservative variables is adopted (see Bassi et al. (2015)). The jacobian matrix is computed numerically by a finite difference approximation. The solution of the linear system described by Eq.5 is required at each time step and represents the largest cost of the simulation. In this work, the GMRES solver with the ILU0 preconditioner is chosen for this task by calling the PARALUTION library (Lukarski and Trost (2014)).

3. DD-LPOD-DG: Domain Decomposition and Local POD-DG method

In this Section the ROM concepts adopted for this work are illustrated. First of all, the idea of Domain Decomposition in the framework of ROM for fluid dynamics is presented in Section 3.1. Then the use of local POD basess in a DG framework (LPOD-DG) will be introduced in Section 3.2. Finally, the possibility to exploit some features of the LPOD-DG approach to obtain an online adaptive procedure is discussed in Section 3.3.

3.1. *Domain Decomposition*

The application of ROM techniques to fluid dynamics problems is challenging because of the presence of strong non-linearities in the governing equations. For example, phenomena such the advection of vortex structures or travelling shock waves represent difficult obstacles because they cannot be easily described by superposition of effects. In particular, the use of linear approaches to describe these non-linear phenomena requires an extremely fine sampling of the parameter space in the offline phase. A possible alternative approach can be applied in those problems where the non-linearities are localised in a subset of the computational domain: domain decomposition. The idea is that the regions where there are the stronger non-linear phenomena should be studied by means of the high-fidelity solver while the other regions can be described by a low fidelity model. A similar approach can be followed during local shape deformation analysis: if the geometry of the body is locally altered then it is possible to apply the high-fidelity solver only in the neighbourhood of the deformation while a cheaper model can be used elsewhere. An example of this approach for incompressible flows was proposed by Bergmann et al. (2018). In particular, that work suggests to couple the low fidelity and the high-fidelity models by performing a projection over an overlapping region in which both models are defined.
In the present work the domain decomposition approach is exploited in the DG framework: this simplifies the implementation since it avoids the definition of an overlapping region. In particular, the choice between the high-fidelity and the low fidelity model is here traduced in choosing between a standard DG polynomial basis and a smaller POD basis inside each element, as described in the following Section.

3.2. *LPOD-DG approach*

The basic idea of the LPOD-DG approach is to substitute the original DG element basis with an empirical local POD basis obtained from a database of previous high-

fidelity solutions. This procedure is natural in a modal DG framework because different basis can be chosen for different elements. Furthermore, the DG method potentially allows to use a different basis for each conservative variables.
The procedure can be applied in those elements of the mesh which do not change when the body is deformed: this explains why the LPOD-DG approach is strongly linked to domain decomposition.
A description of the LPOD-DG method for compressible flows is available in the work of Ferrero, Iollo, and Larocca (2018). Here the most important features are reported. The key idea is that most of the computational cost of the present discretisation is related to the solution of the linear system reported in Eq. 5. In order to reduce this cost, the size of the global vector is reduced by substituing the original DG basis with the POD local basis in the elements belonging to the fixed mesh region. In this way the global vector of unknows $\tilde{\boldsymbol{Q}} \in \mathbb{R}^{N_{DOF}}$ is substituted by the smaller global vector $\hat{\boldsymbol{A}} \in \mathbb{R}^{N_{DOF}^{POD}}$ and Eq. 5 becomes:

$$[\boldsymbol{M}]\frac{\hat{\boldsymbol{A}}^{n+1} - \hat{\boldsymbol{A}}^{n}}{\Delta t} = \hat{\boldsymbol{R}}(\hat{\boldsymbol{A}}^{n}) + \hat{\boldsymbol{J}}(\hat{\boldsymbol{A}}^{n})(\hat{\boldsymbol{A}}^{n+1} - \hat{\boldsymbol{A}}^{n}), \tag{6}$$

where the global mass matrix $[\boldsymbol{M}]$ is the identity because of the orthonormality of the POD modes. The new size of the problem is given by summing the number of DOF over all the N_T elements:

$$N_{DOF}^{POD} = \sum_{e=1}^{N_T} \sum_{l=1}^{5} \hat{N}_{le} < N_{DOF}, \tag{7}$$

where $\hat{N}_{le}$ is the size of the basis for the l-th conservative variable in the element e.

The previous passages can be seen as just a local adaptation of the element basis. However, it is useful to keep both the original DG basis and the POD basis in all the elements. This choice has two advantages. First of all, the time derivative of the POD degrees of freedom required by Eq. 6 can be evaluated by computing the time derivative of the original DG degrees of freedom and then performing a projection on the POD basis. This simplifies the implementation of the LPOD-DG method in an existing code since it just requires the implementation of a simple projection operator. Furthermore, the computation of the time derivative for the DG degrees of freedom and the projection have a negligible cost with respect to the solution of the linear system reported in Eq. 6.
The second advantage of keeping both bases inside the element is related to the possibility of obtaining a residual-based error indicator which can be used to drive an adaptive procedure at runtime, as explained in the next Section.
It should be noted that the LPOD-DG approach requires to define an empirical POD basis for each governing equation while the standard DG approach uses the same basis for all the equations. This means that the LPOD-DG introduces a memory overhead which could become significant in problems where several governing equations must be integrated (for example in the simulation of chemically reacting flows where transpost equations for several chemical species are integrated).
Furthermore, the use of different basis sizes in the different elements introduces load balancing problems in parallel computations. However, these problems are shared with

p-adaptive schemes and are not critical in steady state problems where the load balancing should be performed only at the beginning of the simulation.

3.3. *Adaptivity*

The steady solution of the LPOD-DG discretisation is found by integrating Eq.6 until the time derivative of the vector $\hat{\boldsymbol{A}}$ reduces under a certain threshold. In the elements of the fixed mesh region where the LPOD-DG approach is applied, the time derivative of the original DG degrees of freedom is also available. If the POD basis described the same space of the original DG basis then also the time derivative of the DG degrees of freedom would be null. However, the POD basis describes a space which is smaller than the original DG space. In those elements where the POD basis is not suitable to describe properly the solution then the time derivative of the DG degrees of freedom can assume large values: they represent a residual-based error indicator.
In particular, it is possible to integrate the LPOD-DG equations until steady state and then evaluate the DG residuals. A simple ranking of the DG element residuals allows to identify the regions where the POD performs poorly. In these elements, the POD basis can be substituted by the original DG basis and the simulation can be restarted from the current solution: since only weak perturbations are introduced in the solution it is generally sufficient to perform a few steps with the implicit scheme to reach a new steady solution.

4. Preliminary validation and convergence study

First of all, the DG solver with the Spalart-Allmaras model is tested on the flow around the T106c gas turbine cascade for which experimental data are available from Michálek, Monaldi, and Arts (2012). This test case represents a significant example of the flow around high-lift blades in low pressure aeronautic gas turbines. The chosen working condition is characterised by the following data: inlet angle $\alpha_1 = 32.7°$, isentropic exit Mach number $M_{2s} = 0.65$ and isentropic exit Reynolds number $Re_{2s} = 250000$. The experimental setup was characterised by an almost laminar inlet condition (the turbulence intensity is approximately equal to 1%): in order to reproduce such a condition, a very low inlet level for the Spalart-Allmaras eddy viscosity is chosen: $\tilde{\nu}/\nu = 0.1$. Periodic boundary conditions are imposed in the vertical direction. An high-order curvilinear grid which contains approximately 5000 elements is generated with Gmsh (Geuzaine and Remacle (2009)). This grid is used to perform a convergence analysis in which the reconstruction order (and so the number of degrees of freedom) is progressively increased up to a fourth order accurate scheme (DG3). In Figure 1 the wall isentropic Mach number distribution is reported. The plot allows to compare the experimental data with the numerical predictions obtained for the different reconstruction orders. The results for $p = 1$ show some oscillations which are typical of DG schemes in the presence of under-resolved boundary layers. These oscillations tend to disappear when the reconstruction order is increased and an almost smooth solution is obtained for $p = 3$. The fact that the solution is strongly under-resolved for $p = 1$ makes the time integration of the equations quite difficult. In order to avoid instabilities during the strong initial transient a filtering stabilisation is applied following the approach proposed by Ferrero and Larocca (2016). The filtering is deactivated after the initial transient and for the higher-order discretisations.
This preliminary mesh dependence analysis which gives results in line with previous

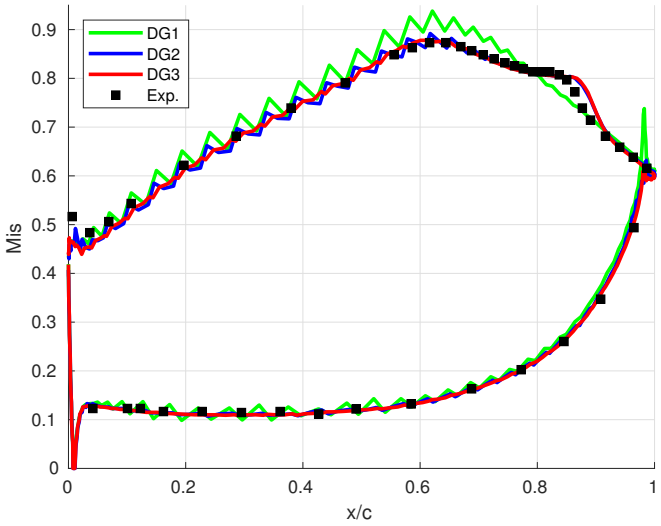

Figure 1. Wall isentropic Mach number distribution for T106c cascade: convergence analysis

studies performed on this blade with other turbulence models (Ferrero, Larocca, and Bernaschek (2017); Ferrero and Larocca (2017)) allows to confirm that the chosen mesh resolution level is sufficient for a DG3 fourth order discretisation. All the simulations reported in the following will be performed with the same mesh resolution level.

5. Blade shape design by means of DD-LPOD-DG

In this Section the Domain Decomposition approach and the LPOD-DG scheme are applied together to the study of the flow around a family of gas turbine profiles. In particular, the influence of the shape of the suction side on the flow field is investigated. In order to describe easily different profiles a parametrisation system is introduced following the approach described by Ampellio et al. (2016). According to this parametrisation, the leading edge and the trailing edge are described by circular arcs. The pressure side and the suction sides are described by third order and fourth order rational Bezier spline, respectively. For each control points it is possible to define three parameters: its coordinates and a weight which represents a measure of the attraction exerted by the control point on the Bezier curve. A scheme which shows the control points and the parametric curves is reported in Figure 2. The obtained parametrisation system is used to fit the geometry of the T106c blade. The shape of the pressure side and the leading and trailing edge arcs will remain fixed for all the following simulations. As far as the suction side is concerned, the position of the first and last points of the spline (P_1 and P_5 in Figure 2) is fixed because these points are determined by the end of the leading edge and trailing edge arcs. Unit weights are assumed for the points P_1 and P_5 and are not changed for all the shapes considered in the following. The position of the points P_2 and P_4 defines the initial and final slope of the spline which must be continuous at the interfaces with the circular arcs. In the following study these points are assumed fixed. However, the weights of the points P_2 and P_4 will be chosen as free parameters to evaluate different shapes in the database.

In the following, these parameters will be identified as W_2 and W_4. The position of the point P_3 is automatically recomputed for each choice of W_2 and W_4 in order to guarantee that the spline passes throught the throat point which was found on the original fitting of the T106 profile. This constraint is important to approximately assure that the mass flow rate which can pass in the channel between two blades remains constant.
A suitable range is chosen for each free parameter in order to explore significantly different shapes. Four profiles at the corners of the parameter space are generated in order to create a database of high-fidelity solutions (DB1). In Figure 3 the parameter space and the shape of the profiles in the database are reported. In Figure 4 the Mach field around the profiles A,B,C and D is shown. Better sampling strategies for the definition of the high-fidelity database are available but uniform sampling is sufficient for the goal of this study.
In Figure 6a an example of computational mesh is reported: it contains two regions. The blue region represents the fixed portion of the mesh which is adjacent to the pressure side and which is the same for all the geometries. In contrast, the red region is characterised by a mesh which changes following the shape of the suction side. In order to obtain always the same point distribution in the blue region even when the suction side changes it is important to avoid the introduction of attractors which depends on the distance from the suction side: the element size distribution is indeed imposed in the Gmsh script by prescribing directly the points distribution along some curves and by using attractors which depend only on geometrical points which belong to the pressure side, the trailing edge arc and the leading edge arc. In the configurations considered in this work, the number of elements in the fixed mesh region represents approximately 75% of the total. The number of elements in the unstructured region generated by Gmsh changes slightly for the different geometries: in the test cases presented in the following the total number of elements in the mesh will be in the range 2800-2900. This value is lower with respect to the mesh size used for the mesh convergence study reported in Section 4 (5000 elements): this is due to the fact that a coarser mesh is now used in the wake region since some numerical tests showed that this choice doesn not alter significantly the accuracy of the wall isentropic Mach number distribution that will be studied in the following.

The database DB1 which contains the high-fidelity solutions A,B,C and D is used to build local POD bases in the elements of the fixed mesh region. The POD bases are truncated after reaching 99% of the Total Information Content which is computed as the sum of all the eigenvalues.
In order to test the prediction ability of the proposed approach a set of 10 random test geometries is generated. The position of the test points in the parameter space is reported in Figure 3. In Figure 6a the degrees of freedom (DOFs) per element distribution is reported for the DD-LPOD-DG approach. The elements in the geometry-dependent mesh region requires 50 DOFs per element (because the DG3 scheme requires 10 DOFs per equation and there are 5 governing equations). However, most of the elements in the fixed mesh region requires just 5 DOFs per element, which means that only one mode is kept for each equation. Slightly larger POD bases can be seen in the wake region. The number of degrees of freeedom in the element POD basis can be related to the POD eigenvalues decay rate: the slower the decay of the eigenvalues, the larger the size of the POD basis required to achieve the chosen level of the Total Information Content.
As a consequence of this DOFs distribution, the implicit integration of the DD-

LPOD-DG simulations can be carried out by solving a linear system which is approximately 3 times smaller with respect to a standard DG3 simulation on the same mesh. Particular care should be dedicated to the initialisation of the LPOD-DG simulations: since the POD basis is less general than the original DG basis it is less robust in describing strong transients. For this reason, the LPOD-DG simulations are initialised by the field obtained by a previous DG0 inviscid simulation which is extremely fast but sufficient to avoid the development of unphysical transients.
The proposed approach is also compared with a simple p-adaptive strategy which is implemented with the following rule. Suppose that the size of the basis required by LPOD-DG scheme for one of the conservative equations in an element is n_{POD}. Then the p-adative scheme must use the smallest basis with size $n_p \geq n_{POD}$ for all the conservative equations in that element. This rule comes from the larger flexibility of the LPOD approach with respect to p-adaptive methods. A first advantage is that the LPOD-DG approach allows to use different basis sizes for different equations while the p-adaptive scheme uses the same basis for all equations. This benefit can be exploited for example in subsonic boundary layers where the LPOD-DG could use a larger basis for momentum and a smaller basis for density.
Another advantage is related to the potential anisotropy of the POD basis. For example, consider again an element in the boundary layer: the LPOD-DG approach could describe the solution in the element by using a single mode which is linear or constant in the streamwise direction and cubic in the wall normal direction. In order to obtain the same accuracy level with a p-adaptive scheme it would be necessary to use a full basis which contains cubic terms in both directions: this means that ten modes would be required to get the same accuracy obtained by the LPOD-DG approach with a single mode.
Finally, the approach used in the present work to compute diffusive fluxes (Ferrero, Larocca, and Puppo (2015)) assumes that the volume integral which appears in the DG formulation is computed by using the gradients of the element solution: in order to obtain the gradients required for the viscous fluxes and the source terms it is necessary to use at least a second order accurate reconstruction (DG1). This means that the p-adaptive scheme must always use at least three degrees of freedom per equation in each element. In constrast, the LPOD-DG approach uses basis functions (POD modes) which are obtained as linear combinations of full order snapshots: for this reason, even a POD basis with a single mode can contain the information required to compute the gradients and so the minimum basis size which can be chosen for the LPOD-DG and the p-adative methods is one and three, respectively.

The accuracy of the predictions is investigated by evaluating the norm-2 error on the wall isentropic Mach number distribution which is compared to a standard DG3 solution. The error is defined as

$$Er = \sqrt{\frac{\int_w (M_{is}^{LF} - M_{is}^{HF})^2 dl}{\int_w dl}}, \tag{8}$$

where w identifies the wall boundary and the superscript HF and LF refer to the reference DG3 and the DD-LPOD-DG solutions, respectively. The error obtained on the ten prediction points is reported in Figure 5a as a function of the total number of degrees of freedom. The wall isentropic Mach number distribution of the worst prediction (test T1) is also shown in Figure 5b.

A second set of predictions is performed by using POD bases generated from the database DB2 which is obtained by a 3×3 sampling of the parameter space (see DB2 in Figure 3). The results in Figure 5 show that, in the present configuration, the enrichment of the database does not introduce a clear improvement.
Instead of augmenting the offline cost by adding further high-fidelity solutions in the database, an alternative approach is investigated. In particular, the availability of both the POD and DG3 basis in the fixed mesh region gives indications on which are the elements where the POD basis introduces large errors, as explained in Section 3.3. In this way, it is possible to perform a preliminary DD-LPOD-DG simulation with the POD basis in all the elements belonging to the fixed mesh region and then substitute the POD basis with the standard DG3 basis in those elements where the POD basis gives poor results. In particular, 10% and 20% of the elements with the largest residuals are adapted with this approach: the results reported in Figure 5 show a significant reduction in the prediction error. The DOF distribution for the adaptive discretisations is reported in Figure 6. The map shows clearly that the adaptation takes place in the leading edge region and in the wake.
The results obtained by the p-adaptive approach are also reported in Figure 5a: the plot shows that the implemented p-adaptive strategy gives errors comparable to those obtained by the DD-LPOD-DG approach but with a larger number of degrees of freedom.

In Table 1 the number of degrees of freedom and the measured computational cost of the different approaches is reported for one of the prediction tests. Since an implicit time integration scheme is used the main contributions to the simulation time come from the computation of the jacobian matrix (which is performed numerically, as reported by Ferrero, Iollo, and Larocca (2018)) and from the solution of the linear system by GMRES. The results reported in the table refer to a single jacobian evaluation and a single GMRES solution (with a maximum number of iterations set to 1000, Krylov subspace size set to 200, relative tolerance on the residual set to 10^{-8}) obtained on a single core. The computational time required to project the DG residuals on the POD basis and vice-versa (required by the LPOD-DG approach) is negligible ($\approx 2 \cdot 10^{-2}$ s). Furthermore, the projection operation is trivially parallelisable since it is performed element-wise.
The results in the Table show that the LPOD-DG approach introduces a significant reduction in the computational cost with respect to the full order DG3 scheme.

	NDOF	CPU Time Jacob.[s]	CPU Time GMRES[s]
DG3	142950	11.9	16.7
DD-LPOD-DG (DB1)	49010	3.97	4.00
DD-LPOD-DG (DB2)	49000	4.04	4.01
DD-LPOD-DG adapt.10%	61786	4.98	5.73
DD-LPOD-DG adapt.20%	74588	6.45	7.06
DG p-adapt.	69625	5.00	5.77

Table 1. Computational cost for different approaches

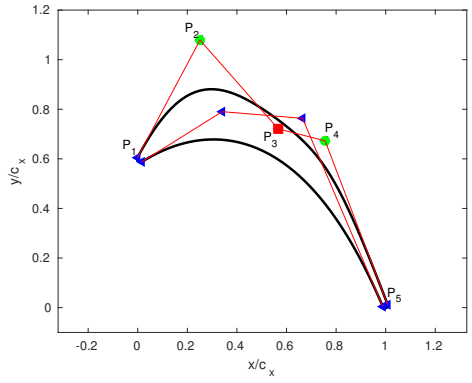

Figure 2. Airfoil parameterization with Bezier splines and circular arcs

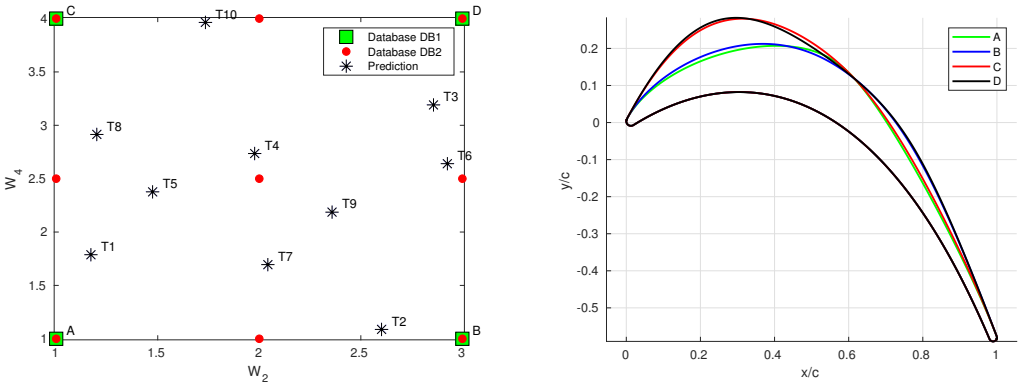

(a) Parameter space (b) Shapes in the database DB1

Figure 3. Database and test geometries

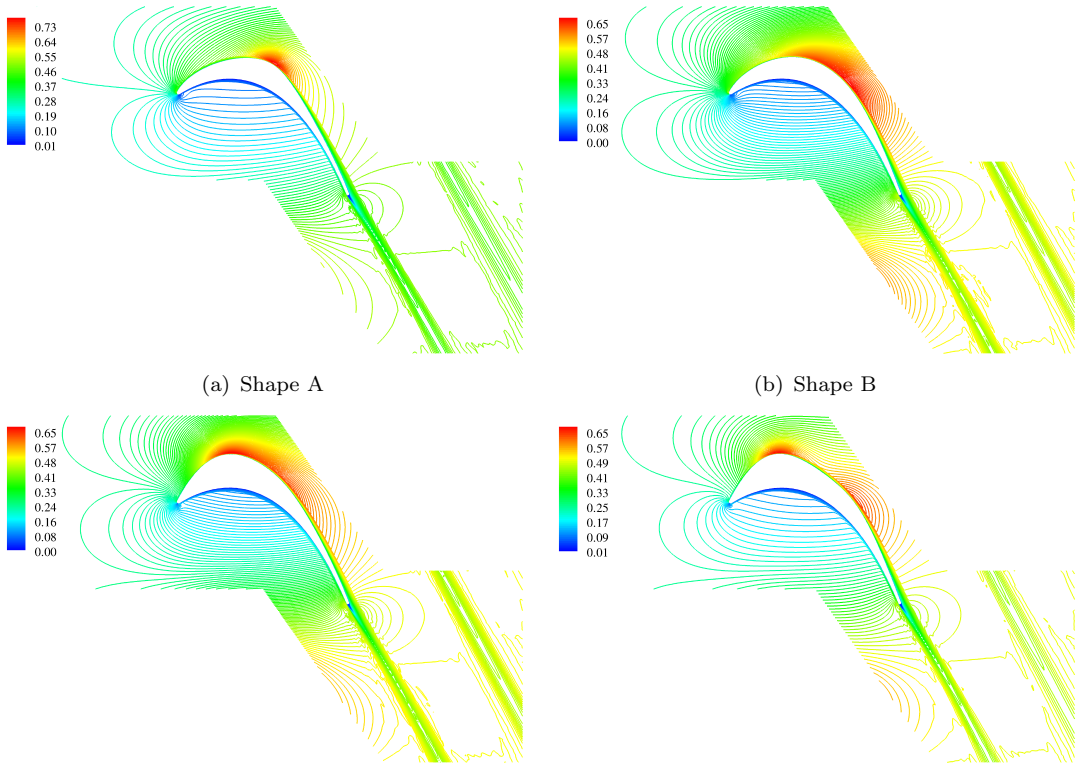

(a) Shape A (b) Shape B

(c) Shape C (d) Shape D

Figure 4. Mach field for the airfoil A, B, C and D in the database DB1 (DG3 solution)

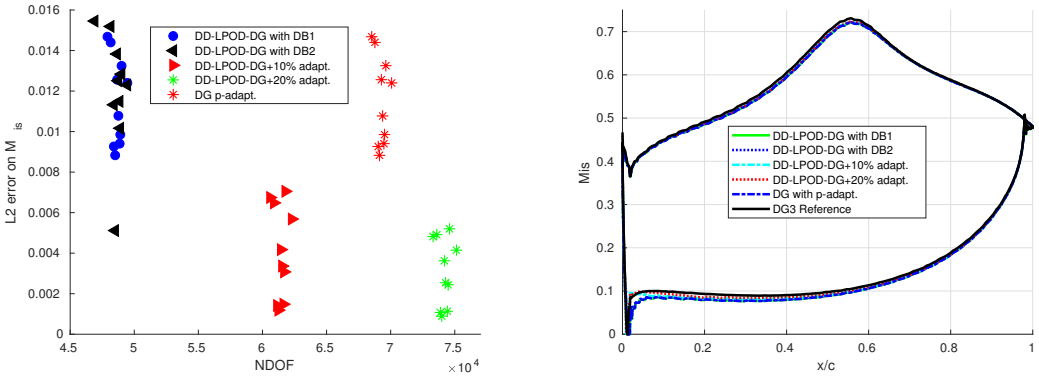

(a) DD-LPOD-DG prediction error (b) Detail of predictions on test T1

Figure 5. Prediction error for test geometries

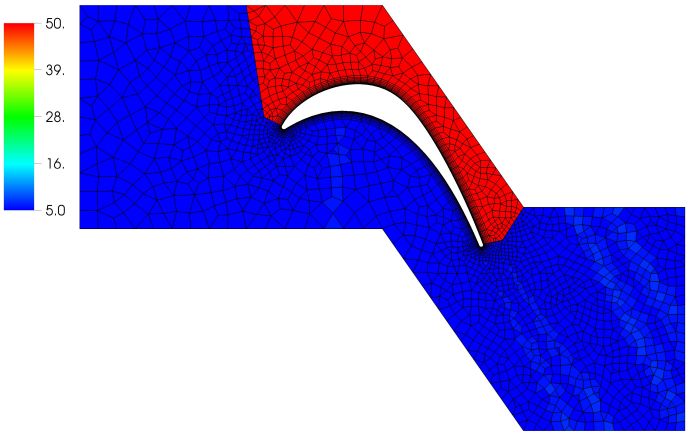

(a) Original DOF distribution

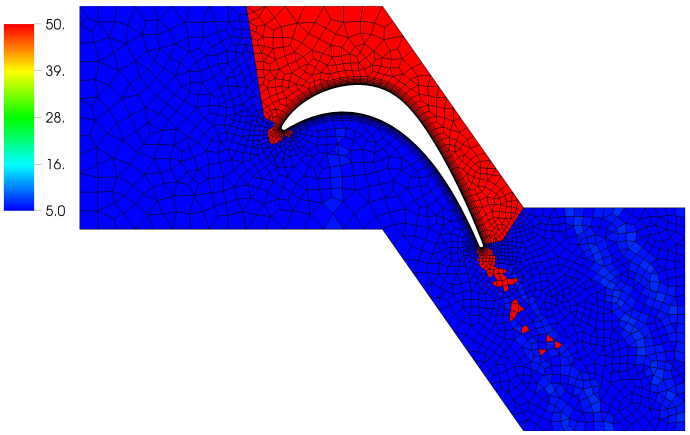

(b) DOF distribution after adaptation of 10% of the elements

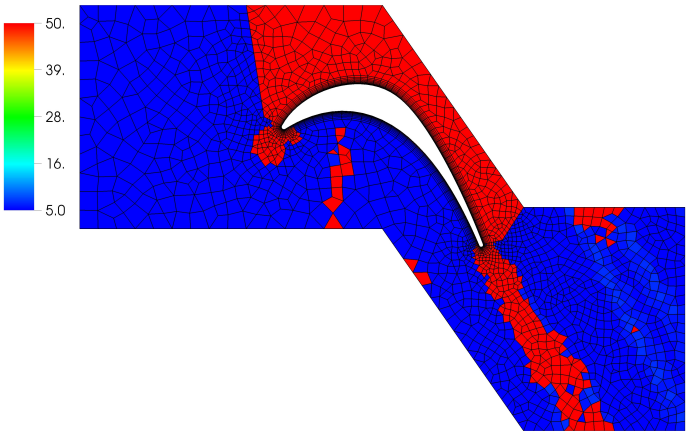

(c) DOF distribution after adaptation of 20% of the elements

Figure 6. Degrees of freedom (DOF) per element distribution with DD-LPOD-DG method

6. Conclusions

Two different ROM techniques are proposed together for accelerating the simulation of the compressible turbulent flow around a family of gas turbine profiles: domain decomposition and LPOD-DG method. Domain Decomposition allows to take advantage of local changes in the body geometry by defining an high fidelity region and a low fidelity region. The LPOD-DG approach offers the possibility to significantly reduce the cost of the problem by introducing local POD basis which substitutes the original larger DG basis. In the 2D problem studied in this work the proposed techniques allows to reduce the size of the linear system required by the implicit integration by a factor 3. Greater benefits could be expected in 3D problems for turbomachinery flows: for example, shape optimisation studies devoted to the reduction of tip clearance effects or hub secondary flows could obtain great benefits since the LPOD-DG approach could be applied in most of the domain.
The LPOD-DG approach is also compared with a simple p-adaptive strategies in order to put in evidence some differences between the two approaches. In particular, while the p-adaptive approach uses the same basis for all the conservative equations, the LPOD-DG approach uses a different basis for each equation. Furthermore, the POD modes are potentially anisotropic and can contain high order terms only in specific directions defined by the physics of the flow (for example in the boundary layer region) while the bases used in classical p-adaptive schemes are isotropic and so they must include all high order terms, also for directions in which the solution does not change significantly.
Finally, an automatic adaptive technique is proposed to improve the predicted LPOD-DG solution at run-time by using a residual-based error indicator. This approach is general and does not require the introduction of problem-dependent criteria.

Acknowledgement

Computational resources were provided by HPC@POLITO (http://www.hpc.polito.it).
Some experiments presented in this paper were carried out using the PLAFRIM experimental testbed, being developed under the Inria PlaFRIM development action with support from Bordeaux INP, LABRI and IMB and other entities: Conseil Régional d'Aquitaine, Université de Bordeaux and CNRS (and ANR in accordance to the programme Investissements d'Avenir (see https://www.plafrim.fr/).

References

Aletti, Matteo C, Simona Perotto, and Alessandro Veneziani. 2018. "HiMod Reduction of Advection–Diffusion–Reaction Problems with General Boundary Conditions." *Journal of Scientific Computing* 76 (1): 89–119.

Allmaras, Steven R, and Forrester T Johnson. 2012. "Modifications and clarifications for the implementation of the Spalart-Allmaras turbulence model." In *Seventh international conference on computational fluid dynamics (ICCFD7)*, 1–11.

Ampellio, Enrico, Francesco Bertini, Andrea Ferrero, Francesco Larocca, and Luca Vassio. 2016. "Turbomachinery design by a swarm-based optimization method coupled with a CFD solver." *Advances in aircraft and spacecraft science* 3 (2): 149–170.

Amsallem, David, and Charbel Farhat. 2008. "Interpolation method for adapting reduced-order models and application to aeroelasticity." *AIAA journal* 46 (7): 1803–1813.

Amsallem, David, Matthew Zahr, Youngsoo Choi, and Charbel Farhat. 2015. "Design optimization using hyper-reduced-order models." *Structural and Multidisciplinary Optimization* 51 (4): 919–940.

Bai, Zhe, Steven L Brunton, Bingni W Brunton, J Nathan Kutz, Eurika Kaiser, Andreas Spohn, and Bernd R Noack. 2017. "Data-driven methods in fluid dynamics: Sparse classification from experimental data." In *Whither Turbulence and Big Data in the 21st Century?*, 323–342. Springer.

Baiges, Joan, Ramon Codina, and Sergio Idelsohn. 2013. "A domain decomposition strategy for reduced order models. Application to the incompressible Navier–Stokes equations." *Computer Methods in Applied Mechanics and Engineering* 267: 23–42.

Baroli, Davide, Cristina Maria Cova, Simona Perotto, Lorenzo Sala, and Alessandro Veneziani. 2017. "Hi-POD solution of parametrized fluid dynamics problems: preliminary results." In *Model Reduction of Parametrized Systems*, 235–254. Springer.

Barrault, Maxime, Yvon Maday, Ngoc Cuong Nguyen, and Anthony T Patera. 2004. "An 'empirical interpolation' method: application to efficient reduced-basis discretization of partial differential equations." *Comptes Rendus Mathematique* 339 (9): 667–672.

Bassi, Francesco, L Botti, Alessandro Colombo, Andrea Crivellini, Nicoletta Franchina, Antonio Ghidoni, and Stefano Rebay. 2010. "Very high-order accurate discontinuous Galerkin computation of transonic turbulent flows on aeronautical configurations." In *ADIGMA-A European Initiative on the Development of Adaptive Higher-Order Variational Methods for Aerospace Applications*, 25–38. Springer.

Bassi, Francesco, L Botti, Alessandro Colombo, Andrea Crivellini, Antonio Ghidoni, Alessandra Nigro, and Stefano Rebay. 2015. "Time integration in the discontinuous galerkin code MIGALE-Unsteady problems." In *IDIHOM: Industrialization of High-Order Methods-A Top-Down Approach*, 205–230. Springer.

Bassi, Francesco, Lorenzo Botti, Alessandro Colombo, Daniele A Di Pietro, and Pietro Tesini. 2012. "On the flexibility of agglomeration based physical space discontinuous Galerkin discretizations." *Journal of Computational Physics* 231 (1): 45–65.

Bergmann, Michel, Andrea Ferrero, Angelo Iollo, Edoardo Lombardi, Angela Scardigli, and Haysam Telib. 2018. "A zonal Galerkin-free POD model for incompressible flows." *Journal of Computational Physics* 352: 301–325.

Bertram, Anna, Carsten Othmer, and Ralf Zimmermann. 2018. "Towards Real-time Vehicle Aerodynamic Design via Multi-fidelity Data-driven Reduced Order Modeling." In *2018 AIAA/ASCE/AHS/ASC Structures, Structural Dynamics, and Materials Conference*, 0916.

Buffoni, Marcelo, Haysam Telib, and Angelo Iollo. 2009. "Iterative methods for model reduction by domain decomposition." *Computers & Fluids* 38 (6): 1160–1167.

Chaturantabut, Saifon, and Danny C Sorensen. 2010. "Nonlinear model reduction via discrete empirical interpolation." *SIAM Journal on Scientific Computing* 32 (5): 2737–2764.

Chinesta, Francisco, Roland Keunings, and Adrien Leygue. 2013. *The proper generalized decomposition for advanced numerical simulations: a primer*. Springer Science & Business Media.

Ferrero, Andrea, Angelo Iollo, and Francesco Larocca. 2018. "Global and local POD models for the prediction of compressible flows with DG methods." *International Journal for Numerical Methods in Engineering* 116 (5): 332–357.

Ferrero, Andrea, and Francesco Larocca. 2016. "Feedback filtering in discontinuous Galerkin methods for Euler equations." *Progress in Computational Fluid Dynamics, an International Journal* 16 (1): 14–25.

Ferrero, Andrea, and Francesco Larocca. 2017. "Adaptive CFD schemes for aerospace propulsion." *Journal of Physics: Conference Series* 841 (1).

Ferrero, Andrea, Francesco Larocca, and Verena Bernaschek. 2017. "Unstructured discretisation of a non-local transition model for turbomachinery flows." *Advances in aircraft and spacecraft science* 4 (5): 555–571.

Ferrero, Andrea, Francesco Larocca, and Gabriella Puppo. 2015. "A robust and adaptive recovery-based discontinuous Galerkin method for the numerical solution of convection–diffusion equations." *International Journal for Numerical Methods in Fluids* 77 (2): 63–91.

Geuzaine, Christophe, and Jean-François Remacle. 2009. "Gmsh: A 3-D finite element mesh generator with built-in pre-and post-processing facilities." *International journal for numerical methods in engineering* 79 (11): 1309–1331.

Gibou, Frederic, David Hyde, and Ron Fedkiw. 2018. "Sharp interface approaches and deep learning techniques for multiphase flows." *Journal of Computational Physics* .

Lukarski, Dimitar, and Nico Trost. 2014. "PARALUTION project." *URL http://www. paralution. com. Accessed: December* .

Michálek, Jan, Michelangelo Monaldi, and Tony Arts. 2012. "Aerodynamic performance of a very high lift low pressure turbine airfoil (T106C) at low Reynolds and high Mach number with effect of free stream turbulence intensity." *Journal of Turbomachinery* 134 (6): 061009.

Mohebujjaman, M, LG Rebholz, and T Iliescu. 2018. "Physically constrained data-driven correction for reduced-order modeling of fluid flows." *International Journal for Numerical Methods in Fluids* .

Noack, Bernd R, Witold Stankiewicz, Marek Morzyński, and Peter J Schmid. 2016. "Recursive dynamic mode decomposition of transient and post-transient wake flows." *Journal of Fluid Mechanics* 809: 843–872.

Pandolfi, Maurizio. 1984. "A contribution to the numerical prediction of unsteady flows." *AIAA journal* 22 (5): 602–610.

Quarteroni, Alfio, and Gianluigi Rozza. 2014. *Reduced order methods for modeling and computational reduction*. Vol. 9. Springer.

Quarteroni, Alfio, Gianluigi Rozza, and Andrea Manzoni. 2011. "Certified reduced basis approximation for parametrized partial differential equations and applications." *Journal of Mathematics in Industry* 1 (1): 3.

Salmoiraghi, F., A. Scardigli, H. Telib, and G. Rozza. 2018. "Free-form deformation, mesh morphing and reduced-order methods: enablers for efficient aerodynamic shape optimisation." *International Journal of Computational Fluid Dynamics* 32 (4-5): 233–247. https://doi.org/10.1080/10618562.2018.1514115.

Schmid, Peter J. 2010. "Dynamic mode decomposition of numerical and experimental data." *Journal of fluid mechanics* 656: 5–28.

Sirovich, Lawrence. 1987. "Turbulence and the dynamics of coherent structures part I: coherent structures." *Quarterly of applied mathematics* 45 (3): 561–571.

Swischuk, Renee, Laura Mainini, Benjamin Peherstorfer, and Karen Willcox. 2018. "Projection-based model reduction: Formulations for physics-based machine learning." *Computers & Fluids* .

Tezzele, Marco, Filippo Salmoiraghi, Andrea Mola, and Gianluigi Rozza. 2018. "Dimension reduction in heterogeneous parametric spaces with application to naval engineering shape design problems." *Advanced Modeling and Simulation in Engineering Sciences* 5 (1): 25.

Weller, Jessie, Simone Camarri, and Angelo Iollo. 2009. "Feedback control by low-order modelling of the laminar flow past a bluff body." *Journal of Fluid Mechanics* 634: 405–418.